

1. Introduction

Identifying the source regions of the solar wind is important both as a fundamental issue in solar physics (Antiochos *et al.*, 2012) and from the space environment perspective (e.g., Luhmann *et al.*, 2002, and references therein). This practice dates back to the era when the solar wind was first measured (Snyder and Neugebauer, 1966; Nolte and Roelof, 1973; Neugebauer *et al.*, 1998, see also Poletto 2013 for a historic overview). With the solar wind data accumulated throughout several solar activity cycles in both near-ecliptic and polar orbits, scenarios have emerged as to how the solar wind sources evolve with solar activity. This concerns not only the solar winds sampled by individual spacecraft but also the solar winds throughout the heliosphere (Luhmann *et al.*, 2002).

Traditionally, the studies on the solar wind sources start with categorizing the winds into the fast (with proton speeds v over, say, 500 km s^{-1}) and slow ones ($v \lesssim 500 \text{ km s}^{-1}$) (e.g., Schwenn, 2006). Regarding the fast solar wind (FSW), the coronal source is generally accepted to be coronal holes (e.g., Krieger, Timothy, and Roelof, 1973; Zirker, 1977; Gosling and Pizzo, 1999). Tracing the wind sampled by *Pioneer VI* and *Vela*, Krieger, Timothy, and Roelof (1973) were the first to associate the FSW with a coronal hole. Then Zirker (1977) suggested that all coronal holes are sources of the FSW. Using the SOHO/SUMER data, the outflows at the base of polar (Hassler *et al.*, 1999) and equatorial (Xia, Marsch, and Curdt, 2003) coronal holes were measured, with the results supporting the notion that the FSW originates in coronal funnels (Tu *et al.*, 2005). On the other hand, while examining the ACE and *Ulysses* data for four Carrington rotations during the Cycle 23 maximum, Neugebauer *et al.* (2002) concluded that a fraction of the FSW originate also from active regions.

The sources of the slow solar wind (SSW) are substantially more complex. While there exists the consensus that the SSWs are associated with coronal streamers, debates remain as to exactly where in or around streamers the SSWs originate. The scenario proposed for solar minimum conditions by Wang *et al.* (1998) suggests that there are two kinds of SSWs, with one originating from streamer stalks and the other from just inside coronal holes and immediately adjacent to streamers. The former source is consistent with the outmoving plasmoids found by SOHO/LASCO (Sheeley *et al.*, 1997; Wang *et al.*, 1998), while the latter source is corroborated by the SOHO/UVCS measurements (Abbo *et al.*, 2010) and consistent with the established inverse correlation of the flow tube expansion with the solar wind speed (Wang and Sheeley, 1990). However, even at solar minimum, this scenario remains to be complemented with the expected source of the SSWs from inside streamers, either via direct flow of the plasma from the magnetically open fields in streamer cores (Noci *et al.*, 1997) or via the evaporation of plasmas from the magnetic arcades in streamer helmets (Suess *et al.*, 1999, also Li *et al.*, 2005). Besides, using the method of interplanetary scintillation (IPS) tomographic analysis, Kojima *et al.* (1999) found that yet another SSW source is the unipolar regions in the vicinity of active regions (ARs). A further and more direct study associating the SSW with ARs comes with Hinode X-ray and EUV spectral observations, where the edge of ARs was shown to host persistent upflows with speeds reaching 100 km s^{-1}

(Harra *et al.*, 2008), which may account for up to 1/4 of the in situ SSW (Sakao *et al.*, 2007) provided that these upflows eventually turn into outflows. Indeed, van Driel-Gesztelyi *et al.* (2012) (also see Culhane *et al.*, 2014 and Mandrini *et al.*, 2014) showed that these upflows may access coronal magnetic fields that open into interplanetary space. In addition, using X-ray high temporal-spatial resolution images, Subramanian, Madjarska, and Doyle (2010) found that the magnetic reconnection of co-spatial open and closed magnetic field lines at coronal hole boundaries creates the necessary conditions for plasmas to flow to large distances. This provides an explanation for largely-blue-shifted events observed with EIS/Hinode (Madjarska *et al.*, 2012), indicating these plasma outflows are also a possible SSW source. Comparing the remote sensing and in situ measurements, Feldman, Landi, and Schwadron (2005) suggested that the SSW may also arise from the quiet Sun. When it comes to solar maximum conditions, SSWs are found to originate from small coronal holes and active regions where open magnetic field lines exist (Neugebauer *et al.*, 2002; Wang and Sheeley, 2003; Liewer, Neugebauer, and Zurbuchen, 2004; Ko *et al.*, 2006; Schwenn, 2006; Wang, Ko, and Grappin, 2009)

While the identified coronal sources of the solar wind are diverse, there seem to be an agreement on the approaches behind the identification procedure. First, unlike the solar wind speed itself, ionic charge states, especially those of oxygen and carbon, are suggested to be a telltale signature of the wind sources. Take oxygen for example. The abundance ratio O^{7+}/O^{6+} measured in the in situ solar wind is generally accepted to reflect the electron temperature in the coronal sources, given that it does not vary with distance beyond a fraction of a solar radius above the solar surface (Owocki, Holzer, and Hundhausen, 1983; Büergi and Geiss, 1986; Hefti *et al.*, 2000; Landi *et al.*, 2012b). Now that the temperatures are different in different coronal regions, a comparison of the in situ charge states then allows one to associate the in situ wind with a particular coronal source (e.g., Zurbuchen *et al.*, 2000; Zurbuchen, 2001; Landi *et al.*, 2012a). With this spirit, Zhao, Zurbuchen, and Fisk (2009) divided the non-transient solar winds into two categories: those from coronal holes (CH winds) and those from outside coronal holes (non-CH winds) with O^{7+}/O^{6+} values lower and higher than 0.145, respectively. As a result, about 42% of the ecliptic solar wind was found to be of non-CH origin during 1998-2008. Second, a model of coronal magnetic field is often indispensable. For this purpose, while sophisticated Magnetohydrodynamic (MHD) models are sometimes adopted (Abbo *et al.*, 2010), the potential-field-source-surface model (PFSS) and its variants have been in much wider use. On the one hand, this practice established the long-term trend of the wind speed being inversely correlated with the lateral expansion of the flow tubes (Wang and Sheeley, 1990). On the other hand, applying the PFSS model with an archive of the synoptic magnetogram data leads Luhmann *et al.* (2002) to the distribution of sources of the heliospheric solar wind as a function of solar activity for nearly three activity cycles. In particular, Luhmann *et al.* (2002) found that although polar coronal holes exist for more than 80% of a solar cycle, they contribute to the ecliptic solar winds significantly only during half of a cycle. During the other half of a cycle, the near-ecliptic winds originate from mid- and low-latitude sources instead.

Given the diversity of the wind sources and the complexity of the activity-dependence of these sources during a solar activity cycle, the present study is intended to examine, in a statistical manner, the fractions taken up by the in situ solar winds from various sources from the activity maximum to minimum in Cycle 23. To this end, we start with the *in situ* wind speed measurements, and adopt the standard two-step mapping procedure (Neugebauer *et al.*, 1998, 2002; Liewer, Neugebauer, and Zurbuchen, 2004) to trace the winds to their footpoints at the solar surface. We then examine the corresponding coronal images recorded by SOHO/EIT as well as photospheric magnetograms, and ask the question where the footpoints are located: are they located in a coronal hole (CH), an active region (AR), or the quiet Sun (QS)? The solar winds are therefore grouped accordingly, enabling us to address the question how their in situ properties differ and evolve with different activity levels.

Our study differs from previous studies with similar objectives or similar approaches in the following aspects. First, the approach combining a footpoint tracing method with the context of coronal images follows closely the one in Liewer, Neugebauer, and Zurbuchen (2004), which is in turn built on Neugebauer *et al.* (1998, 2002) where the imaging data were not used. However, while Neugebauer *et al.* (1998) focused on the Cycle 22–23 minimum, and Liewer, Neugebauer, and Zurbuchen (2004, also Neugebauer *et al.* 2002) concerned the Cycle 23 maximum, we examine the solar wind dataset that spans the interval from 1999 to 2008 in which the declining phase and Cycle 23–24 minimum are included. Furthermore, the solar winds from sources other than CHs and ARs are paid attention to, and are classified as the QS winds. Second, both this study and the one by Zhao, Zurbuchen, and Fisk (2009) (ZZF09 hereafter) have similar objectives in examining the distribution of wind sources in response to solar activity. However, the approach for identifying the sources in this study is different from the one by ZZF09 where the O^{7+}/O^{6+} values are a primary discriminator. We note that, given the uncertainties in both approaches, the results of this study are meant not to be contrasted with but rather to complement ZZF09, with the hope that new light can be shed on the sources of the near-ecliptic solar winds. Third, while both using the PFSS model and being statistical in nature, our study differs from the one by Luhmann *et al.* (2002) in that we also employ the imaging as well as magnetogram data to classify the sources instead of using the locations relative to the equator as in Luhmann *et al.* (2002). Fourth, given the considerable interest in and the complexities associated with the sources of the slow solar wind, we will analyze the ACE solar winds in general, and examine the slow ones in particular. In Section 2, we describe the data and our method of analysis. The results are then given in Section 3. Section 4 summarizes the present study, ending with some concluding remarks.

2. Data and analysis

The two-step mapping procedure used in the present study closely follows the one in Neugebauer *et al.* (1998, 2002); Liewer, Neugebauer, and Zurbuchen (2004). To initiate the procedure, we use daily averages of the solar wind speed

made with the *Solar Wind Electron, Proton, and Alpha Monitor* (SWEPAM, McComas *et al.*, 1998) on board the *Advanced Composition Explorer* (ACE, Stone *et al.*, 1998). Also used are the daily averages of the abundance ratios O^{7+}/O^{6+} recorded by the *Solar Wind Ion Composition Spectrometer* (SWICS, Gloeckler *et al.*, 1998), and the magnetic field measurements with the *Magnetic Field Experiment* (MAG, Smith *et al.*, 1998). Given that we are interested in the non-transient solar winds, one immediate purpose for using the O^{7+}/O^{6+} ratios is to eliminate from the ACE dataset those intervals occupied by interplanetary *Coronal Mass Ejections* (ICMEs). To do this, we adopt the same approach as in ZZF09 (see also Richardson and Cane, 2004) whereby we discard the data with O^{7+}/O^{6+} ratios exceeding $6.008 \exp(-0.00578v)$, in which v is the wind speed in km s^{-1} . A detailed analysis by ZZF09 shows that this criterion adequately separates ICMEs from the non-transient ambient winds, being reliable in 83.2% of the cases examined therein. The *in situ* data used in this study span the years between 1999 and 2008, hence encompassing nearly half of the Cycle 23.

The mapping procedure involves two steps. First, the loci of the solar winds are found on the source surface, placed at a heliospheric distance of $2.5 R_{\odot}$ as implemented by the coronal magnetic field model. This is done via a ballistic approach, whereby the longitude correction due to solar rotation is determined by the time for a wind parcel to travel from the source surface to the spacecraft. Here a constant wind speed is used, and assumed to be the one measured by ACE/SWEPAM. The wind parcel is then traced from the source surface to the photosphere by following the magnetic field lines computed by using a PFSS model, provided in the PFSS package as part of the Solar Software. Instead of using the synoptic magnetograms as was done in e.g., Neugebauer *et al.* (1998), this package uses, as the boundary data, the magnetograms measured with SOHO/MDI which are updated every 6 hours. It outputs the magnetic field vector on a $39 \times 384 \times 192$ grid in spherical coordinates inside the source surface (for details, see Schrijver and De Rosa, 2003). It should be noted that as implied by the mapping procedure, the magnetic polarity at the field line footpoint needs to be checked against the one measured *in situ*. Schrijver and De Rosa (2003) found that during 1997-2001, 83% of footpoint polarities matched the interplanetary magnetic field (IMF) measurements at the Earth. In this work, we find a similar behavior: the footpoint polarities are consistent with what is measured by ACE/MAG in 81% of the data from 1999 to 2008. To ensure consistency, we do not include in our further analysis those dates when the polarities at the two ends of the mapping procedure do not match. Table 1 presents, as a function of time, the number of daily samples of the non-transient solar wind (second column, labeled “All sources”), which is sub-divided into the counts of the solar winds from CHs (third column), ARs (fourth), QS (fifth), and Undefined sources (sixth). Given in the parentheses are the numbers that correspond to the cases where the magnetic polarities match. In total, during 1999-2008, 2124 samples are examined in our further analysis, among which 615 (803, 425) samples are associated with CHs (ARs, the QS). One can see that a significant mismatch takes place in 2007 and 2008. This is possibly understandable given that, close to the cycle minimum, the ACE spacecraft was close to the heliospheric current sheet. When mapping the winds to the source surface, a small uncertainty may

lead to a wrong polarity. For future reference, Table 2 presents the comparison between the footpoint polarity and the in situ one for the slow solar winds with speeds lower than 500 km s^{-1} .

The footpoints are then placed in the context of photospheric magnetograms and the EUV images taken by the *Extreme ultraviolet Imaging Telescope* (EIT, Delaboudinière *et al.*, 1995) onboard SOHO (*Solar and Heliospheric Observatory*, Domingo, Fleck, and Poland, 1995). While EIT operates at a number of passbands (Fe IX/X 171 Å, Fe XII 195 Å, Fe XV 284 Å and He II 304 Å), we choose the 284 Å one because the images recorded in this passband reflect the corona at the highest altitude such that coronal holes are more visible. In this passband, EIT takes full-Sun images with a pixel size of $2.6''$ four times a day. For consistency, the field line footpoints are compared with images taken at around 13:00 UT on the day corrected for the wind travel time.

The classification scheme is illustrated in Figure 1, where the EIT images (the left column) are overplotted with the footpoint locations represented by the red crosses. The photospheric magnetograms, on which our scheme also relies, are derived from the PFSS model and given in the right column. The scheme is detailed as follows.

A quantitative approach for identifying coronal hole boundaries is implemented, and the winds that have footpoints located within the hence identified coronal holes (CHs) are classified as “CH winds” accordingly. This approach, which largely follows that in Krista and Gallagher (2009) and Ko *et al.* (2014), is illustrated in Figure 2. If a footpoint is located inside or close to an apparently dark area, then a rectangular box (the white box in Figure 2a) is chosen to enclose this part of the dark region and its surrounding area. An intensity histogram is constructed, and a multi-peak distribution is then obvious (Figure 2c). The well-defined minimum between the first two peaks then defines the threshold for identifying the CH boundary (see the contours in Figure 2a, also Figure 2b, which is the enlarged version of the part inside the box). On the one hand, this scheme enables one to objectively define CH boundaries using the EUV images in only one passband; on the other hand, it is not influenced by the variation of coronal emissions with solar activity.

A description of some technical details for implementing this scheme seems necessary. In practice, we started with asking the question whether there is a dark region close to the traced-back footpoint. By “close”, we mean roughly “within 100 arcsecs”. If the answer is Yes, we then draw a rectangular box, varying in size but typically a few hundred arcsecs across, which encloses both a substantial part of the dark region and its surrounding area. The footpoint is always within this box. It turns out as long as the box is sufficiently large, its size does not significantly influence what one identifies as CH boundaries, for the minima in the different histograms pertinent to different box sizes do not differ substantially. If the answer is NO, we visually choose the dark area that is the closest to the footpoint, and use the same approach to delineate the CH boundary (see e.g., Figure 1d1). If there is no large apparent EUV CH altogether, then we use the threshold found for some obvious CH one or a few days prior to this particular day (An example is shown in Figure 1b1, where the CHs near the two poles are contaminated so significantly that the minimum between the

first two peaks in the intensity histogram can hardly be discerned). The box is substantially smaller than the disc size, we nonetheless use the threshold to delineate CH boundaries throughout the entire solar disc. A space-dependent threshold may be more accurate for mapping CH boundaries on the entire disc, but our approach suffices given that our purpose is to examine whether the footpoint is located inside a CH. Besides, as illustrated by Figure 2a, while a single threshold is adopted, the contours outside the box (the dotted lines) also outline CHs rather accurately.

Our association of a footpoint with an Active Region (AR) or the quiet Sun (QS) relies on the magnetic morphology of the photospheric regions embodying the identified footpoints. The most obvious features on the photosphere are magnetic clusters, which are tentatively named “magnetically concentrated area (MCA)”. Intuitively speaking, MCAs correspond to strong magnetic fields. To make this definition more objective, the absolute value of the radial component of the photospheric magnetic field $|B_{r,\odot}|$ computed from the PFSS model is used. We experimented with different contour levels, $|B_{r,\odot}|_B$, used for outlining MCAs presented in Figure 1 and the attached movie. In practice, if $|B_{r,\odot}|_B$ is assigned a value 1.5 – 4 times the mean of $|B_{r,\odot}|$, then MCAs become well defined. That the MCA morphology is not sensitive to some given $|B_{r,\odot}|_B$, as long as it is in the mentioned range, suggests that MCAs have sharp boundaries. This is understandable considering that MCAs have a strong spatial gradient in $|B_{r,\odot}|$. The thus-defined MCAs encompass all the active regions numbered by NOAA as provided by solarmonitor¹. However, not all MCA patches correspond to a numbered AR. Many of these turn out to correspond to plages with magnetic field weaker than concurrent numbered ARs (see section 3.2 in Zharkova *et al.* 2005). In the three solar activity phases (solar maximum, decline, minimum, see Figure 3) the contour levels are chosen to be 2.0, 2.5, and 3.0 times the mean of $|B_{r,\odot}|$, respectively. In the MAX and DEC phases the threshold is about 10-20 Gs, which is close to the lower bound (15 Gs) adopted by Wang, Ko, and Grappin (2009) to identify slow solar winds from ARs.

With CH boundaries quantitatively defined, when identifying AR and QS sources we need only to concern about the regions outside CHs. An AR source is defined when a footpoint is located inside an MCA that is a numbered AR by NOAA. Likewise, QS sources are defined when a footpoint is located outside any MCA.

With the present grouping scheme, what is unclassified is then named “Undefined”, and corresponds to the case where a footpoint is inside some MCA that is not numbered by NOAA. These sources may be associated with a decaying/developing AR, but it is also possible that they are distinct from AR sources (see, e.g., 06/25-06/27 2005 in the movie where the source is likely a QS one). This is why the word “Undefined” is chosen.

Such a scheme will not overestimate the counts in the respective groups. First, the counts of AR and QS sources are not overestimated, since some footpoints deemed “Undefined” may in fact be AR and QS sources. Second, the counts of

¹<http://solarmonitor.org>

CH winds are not overestimated either, for the current definition of CHs excludes a fraction of CHs with overlying bright emissions. In any case, the counts in the Undefined group account for only a minor fraction of the samples (11.2%, 9.5%, 14.5%, 10.4%, 9.3%, 18.5%, 17.9%, 19.5%, 18.0%, and 5.3% for the years 1999 to 2008, respectively).

Before proceeding, several remarks on our approach seem in order. The first remark is on the reliability of the PFSS model, given its apparently oversimplification of imposing a spherical source surface, neglecting volumetric electric currents between the source surface and the photosphere, and supposing purely radially directed field lines outside the source surface. Nonetheless, a detailed comparison study by Riley *et al.* (2006) demonstrated that the magnetic field configuration computed by the simple PFSS model agrees well with the one found in sophisticated MHD computations, provided that both models are driven by the same line-of-sight magnetograms. From the practical point of view, the magnetically open regions obtained by the PFSS model well match the coronal hole regions identified in, say, the He I 10830 synoptic diagrams (Levine, 1982; Neugebauer *et al.*, 1998, 2002; Schrijver and De Rosa, 2003). A good way to make sure that the traced-back footpoints are reasonably accurate is to compare the current SolarSoft PFSS results with some other calculations. To address this, we randomly chose three Carrington Rotations in the MAX, DEC, and MIN phases, and compared our derived footpoints with those derived from the PFSS model where the magnetogram input is from the Wilcox Solar Observatory (WSO). We found that the fraction of the days when the two different sets of footpoints belong to the same open field region is 80.7% for CR 1969, 84% for CR 2005, and 82.6% for CR 2054. Nevertheless, let us stress that the fraction that the two sets do agree is substantial enough that the statistical study we conduct can be deemed reliable.

Another source of uncertainty may come from the mapping procedure, particularly in view of the simple ballistic treatment involved in the first step. As demonstrated by Nolte and Roelof (1973) (also see Neugebauer *et al.*, 2002), while the solar wind may experience some acceleration beyond the source surface, this effect may be counter-balanced by the near-Sun corotation. Actually a further evidence lending us confidence with this mapping procedure is that, when inspecting the footpoints on a consecutive basis (please see online animation 1 attached to Figure 1), one can see an orderly distribution of the locations of footpoints. They stay in a particular group for several days before moving to another group. In addition, assuming that the uncertainty with the source longitude at the source surface is $\pm 10^\circ$ (Nolte and Roelof, 1973), we select two Carrington rotations in each sub-interval (see Figure 3a) and examine how well our classification scheme works. This is done by tracing the photospheric footpoint from a locus on the source surface 10° eastward or westward of the nominal locus, and then examining whether the footpoint is located in a different area in the EIT images. We found that at maximum activity, about 30% of the footpoints indeed are associated with an area different from what we identified using the nominal locus. During the declining and minimum phases, however, this mismatch reduces to $\lesssim 20\%$ and 10% of the cases examined, respectively.

3. Results

3.1. Sources of the ACE wind between 1999 and 2008

Having categorized the winds, we then address the question of the percentage each kind of wind occupies, and how this evolves in response to solar activity. Figure 3a presents the monthly average of the smoothed sunspot numbers from 1999 to 2008. Three sub-intervals, labeled MAX, DEC and MIN, are then defined according to the level of solar activity. Figure 3b presents the percentage of the CH (shaded blue), AR (red), QS (green) and Undefined (orange) winds in this period. These percentages are yearly averaged values, and add up to unity in each year. One can see that in the sub-interval MAX, the QS supplies only a small fraction of the winds sampled by ACE ($\sim 10\%$), the contributions from CHs is $\sim 15 - 20\%$, and more than half (56%) of the ACE winds originates from ARs. In the declining phase (2002 – 2006), the contributions from CHs and ARs both amount to roughly 34%, and the contributions from ARs (QS) tend to decrease (increase). As for the sub-interval MIN (2007 – 2008), the fraction of the winds from ARs is only marginal ($\lesssim 17\%$), while some 31% comes from the CHs, and nearly half of the winds originates from the QS.

Despite the differences in the approaches for identifying the solar wind sources, Figure 3 agrees with Figure 1 in ZZF09 in that there exists a tendency for coronal sources other than CHs to contribute significantly to the ACE solar winds between 1999 and 2008. Overall, Figure 3b indicates that non-CH sources may be more important than CHs in terms of their mass supply to the solar wind. In particular, Figure 3b indicates that the majority of the near-Earth solar wind comes from ARs during the Cycle 23 maximum. This behavior agrees with ZZF09, and seems to persist to the Cycle 24 maximum as indicated by the very recent study by Brooks, Ugarte-Urra, and Warren (2015). Furthermore, Figure 3 indicates that CH winds tend to dominate in the year of 2003, which is also in line with ZZF09. What is new in Figure 3 is that combining the imaging as well as the magnetogram data allows us to further determine, among the sources outside CHs, the fractions of the winds from ARs and the QS. Some apparent differences from ZZF09 arise as a result. Around the Cycle 23–24 minimum, while ZZF09 indicated that CH winds dominate, our Figure 3b suggests that the contribution from the QS is more important. We stress that this apparent discrepancy stems from the differences in the schemes for classifying the solar winds.

More insights can be gained by examining how the in situ properties of the solar winds categorized by our scheme depend on solar activity. We sort the wind speeds v into 6 bins uniformly spaced between 200 and 800 km s⁻¹, group the O⁷⁺/O⁶⁺ ratios into 6 bins uniformly spaced between 0.0 and 0.6, then present in Figure 4 a contour plot in the v -O⁷⁺/O⁶⁺ space the counts of the winds from different sources as labeled. The left, middle, and right columns correspond to the intervals MAX, DEC, and MIN, respectively. Consider the interval MAX (left column) first. One notices that the majority of the winds corresponds to an O⁷⁺/O⁶⁺ ratio larger than 0.145, which we recall is the criterion that ZZF09 employed to separate CH winds from non-CH ones. However, a more

detailed analysis like ours indicates that not all winds that have O^{7+}/O^{6+} ratios lower than the nominal value of 0.145 are from CHs. Conversely, winds with O^{7+}/O^{6+} exceeding 0.145 are not necessarily non-CH ones. Now consider the years 2007 and 2008, labeled MIN. One can see from Figure 4 (right column) that the O^{7+}/O^{6+} ratios tend to be low, with the majority being lower than 0.145, meaning that if categorizing the ACE winds by this threshold, one would find that nearly all the winds are from CHs. However, combining the footpoint tracing approach with the EUV and magnetic field data, we find that the QS is the primary contributor to the ACE winds during this period. Furthermore, comparing Figures 4c1 with 4c3, one can see that the QS winds are distinct from the CH winds in that they tend to be substantially slower. To select the proper subset of the fast solar wind sampled by ACE that comes from CHs, it would be almost unmistakable to choose those with speeds higher than 600 km s^{-1} and O^{7+}/O^{6+} lower than, say, 0.05. The contamination from the QS winds would be at most marginal, and that from the AR winds would be minimal. We note in passing that this practice has been successfully employed by Zhao and Landi (2014). Regarding the declining phase (middle column of Figure 4), one finds that the possibility of distinguishing between CH winds and non-CH winds lies in between the extremes of maximum and minimum conditions. This is particularly true in the speed dimension. The CH winds tend to be faster than the non-CH ones (mainly from ARs in this case), and the difference between the two tends to be more obvious than for the MAX phase, but appears significantly less obvious than for the MIN phase.

The O^{7+}/O^{6+} ratios for the CH winds during the MAX phase (Figure 4a1) require some explanation. There appears to be a fraction of the CH winds for which the O^{7+}/O^{6+} values exceed 0.26. If assuming ionization equilibrium, this would correspond to a freeze-in temperature exceeding 1.58 MK (Mazzotta *et al.*, 1998). This is beyond the currently accepted electron temperatures derived from remote sensing measurements for CHs below $1.6 R_{\odot}$ (Habbal, Esser, and Arndt, 1993; Esser and Edgar, 2000 and references therein). This apparent discrepancy is not too worrisome given that this fraction of the CH winds tends to originate from the boundaries between CHs and ARs, while the measurements made by Habbal, Esser, and Arndt (1993) pertain to the region well inside a polar CH. Furthermore, as proposed by Esser and Edgar (2000), the electron distribution function may rapidly develop a non-Maxwellian character within the first several solar radii that eventually forms what is measured in situ as the halo electrons (Marsch, 2006). It is worth noting that this non-Maxwellian character is also possible to develop in AR and QS winds.

The differences in the in situ properties of the winds from different sources are further examined in Figure 5, where (a) the wind speed and (b) the oxygen charge state ratio are plotted as a function of time. Given by the green, red, and blue curves are the parameters of the QS, AR, and CH winds, respectively. The standard deviations are given by the error bars for the corresponding values, which are slightly displaced from one another for display purposes. An immediate impression from Figure 5 is that the CH winds tend to be the fastest, while the AR and QS winds have almost the equal speeds. And the O^{7+}/O^{6+} ratios are lowest (largest) for CH (AR) winds, with the QS winds lying in between.

However, the considerable overlap in either the speed or O^{7+}/O^{6+} ranges means that neither of the two parameters, on its own, seems to suffice to discriminate the wind sources. Regarding the activity-dependence of the parameters, one can see from Figure 5a that the wind speeds in the three categories show a similar non-monotonic behavior. Take the CH winds for instance. Their speed start from relatively low values ($\sim 500 \text{ km s}^{-1}$) around MAX, rise to some 590 km s^{-1} in 2003 before decreasing to around 500 km s^{-1} in 2004-2006, and then gradually increase to some 550 km s^{-1} toward the MIN phase. Moving on to Figure 5b, one can see that the overall tendency of O^{7+}/O^{6+} ratios in response to solar activity is opposite to that of the speed, as would be expected given the well-established inverse correlation of the two parameters (Wang and Sheeley, 2003; Wang, Ko, and Grappin, 2009). Nonetheless, one can see that the O^{7+}/O^{6+} ratios from different groups of winds differ more significantly than the speeds do: Note the marked difference in the O^{7+}/O^{6+} values in the CH winds from those in the AR winds in the whole period. It is noteworthy that with decreasing activity, the O^{7+}/O^{6+} ratios in all three types of solar winds tend to decrease, which agrees with Lepri, Landi, and Zurbuchen (2013). The O^{7+}/O^{6+} values in AR (CH) winds are 0.26 (0.16) during MAX, and decrease to 0.10 (0.05) during MIN.

3.2. Sources of the ACE slow wind between 1999 and 2008

Given the considerable interest in understanding the origins of the slow solar wind (SSW), it is informative to apply the same practice to the slow winds alone. In the present study, a SSW is defined to be the wind with speeds lower than 500 km s^{-1} . Figure 6 examines the time evolution of the fractions of the SSWs coming from various sources during 1999-2008. Overall, the impression in the MAX and DEC phases is similar to what one finds in Figure 3 where the solar winds as a whole were considered. This similarity to Figure 3b is not surprising given that, as shown in Figure 4, most of the solar winds is on the lower side when the speed is concerned. During the MIN phase, the contribution from the QS to the slow wind is even more important than that to the overall solar wind. This is also understandable in view of Figure 4c1, given that the solar winds from CHs are largely fast ones.

Figure 7 presents (a) the wind speeds and (b) the O^{7+}/O^{6+} ratios for the slow solar wind as a function of time. As far as the wind speeds are concerned, one can see that the speed in a given group does not show a systematic variation with solar activity. In addition, there is no clear-cut difference in the speeds of the winds from different groups. A stronger temporal variation and a more significant difference in different groups of winds lie in the O^{7+}/O^{6+} values (Figure 7b). Overall, the O^{7+}/O^{6+} values for all the winds show a decrease with decreasing solar activity, and they are substantially different for different groups. The differences in the O^{7+}/O^{6+} values in winds from different sources may be a result of the intrinsic difference in the respective source properties, the magnetic field strength being the most likely one. At any rate, this reinforces the notion raised by Antiochos *et al.* (2012), who suggested that the compositional properties and temporal variability serve better in differentiating the wind sources than the speeds.

The SSW properties may be compared with previous studies. Wang, Ko, and Grappin (2009) suggested that the slow wind during 1998-2007 mainly contains two components: one from small holes located in and around ARs with high O^{7+}/O^{6+} ratios during maximum, the other from the boundaries of large CHs with intermediate O^{7+}/O^{6+} values. Our approach suggests that the majority of the former component indeed comes from ARs during maximum. However, the latter component may actually come from all the three kinds of sources (see Figure 4).

4. Conclusion

The main purpose of this work is to examine, in a statistical sense, the sources of the solar wind sampled by ACE during 1999-2008 in general, and those of the slow solar wind in particular. To this end, we start with the in situ wind speed, and find the photospheric footpoints of the wind parcels by employing the standard two-step mapping procedure (Neugebauer *et al.*, 1998, 2002) where the Potential Field Source Surface (PFSS) model (Schatten, Wilcox, and Ness, 1969; Altschuler and Newkirk, 1969) is used. We then associate the footpoints with various areas in the EUV images recorded by EIT in its 284 Å passband and photospheric magnetograms. With this association we classify the ACE winds into three groups: coronal hole (CH), active region (AR), and quiet Sun (QS) winds. Our main results can be summarized as follows.

- i) During Cycle 23 maximum (years 2000 and 2001), ARs are the main contributor to the ACE winds, the contribution of CHs (QS) is $\sim 20\%$ (13%). The winds in this interval tend to be slow, and the AR winds correspond to substantially higher O^{7+}/O^{6+} values than the CH winds. During the declining phase, the contributions from CHs and ARs both amount to roughly one third. Overall, the fraction of the QS winds in this period is 17%, and tends to increase with decreasing activity, accounting for 31% of the winds in 2006. During the Cycle 23-24 minimum (2007 and 2008), the contribution of CHs (ARs) is about 31% (15%), while the QS contribution is $\sim 41\%$.
- ii) Overall, in each phase of solar activity, the winds from CHs tend to be the fastest and associated with the lowest O^{7+}/O^{6+} ratios. While both lower than CH winds, the speeds of AR and QS winds do not show a substantial difference. A slightly more pronounced difference between AR and QS winds is seen in their O^{7+}/O^{6+} values, with AR winds tending to be slightly hotter. As for the dependence on solar activity of the winds from the same sources, overall with decreasing activity the winds tend to have lower O^{7+}/O^{6+} ratios.
- iii) The fractions occupied by the slow solar winds from different groups show a dependence on solar activity similar to the case where solar winds from all speed ranges are considered. This can also be said for the activity dependence of O^{7+}/O^{6+} values. During the minimum phase, the QS contribution to the slow wind is even more important than its overall contribution, amounting to $\sim 47\%$.

Our results suggest that the quiet Sun is an important source of the ACE solar winds around the cycle 23-24 minimum. A further study dedicated to the examination of the properties of the source region and in situ properties of this particular QS wind is needed. Regarding the source regions, such properties as the magnetic field strength as well as magnetic topology will be of interest. Regarding the in situ properties, the abundances of low first-ionization-potential (FIP) elements relative to their photospheric values will be informative (Feldman, Landi, and Schwadron, 2005; Wang, Ko, and Grappin, 2009). In addition, it will be worthwhile looking for direct signatures of outflow in the QS by examining the Doppler shifts with the emission lines measured with either SOHO/SUMER (e.g., Xia, Marsch, and Curdt, 2003) or Hinode/EIS (e.g., Fu *et al.*, 2014; Brooks, Ugarte-Urra, and Warren, 2015).

Acknowledgments We would like to thank the anonymous referee for helpful comments. We thank the ACE SWICS, SWEPAM, and MAG instrument teams and the ACE Science Center for providing the ACE data. SOHO is a project of international cooperation between ESA and NASA. Wilcox Solar Observatory data used in this study were obtained via the web site <http://wso.stanford.edu> courtesy of J.T. Hoeksema. The Wilcox Solar Observatory is currently supported by NASA. This research is supported by the China 973 program 2012CB825601, the National Natural Science Foundation of China (41174154, 41274176, and 41274178), and the Ministry of Education of China (20110131110058 and NCET-11-0305). BL is also grateful to the International Space Science Institute (ISSI) for providing the financial support to the international team on the origins of the slow solar wind.

References

- Abbo, L., Antonucci, E., Mikić, Z., Linker, J.A., Riley, P., Lionello, R.: 2010, Characterization of the slow wind in the outer corona. *Advances in Space Research* **46**, 1400. DOI. ADS.
- Altschuler, M.D., Newkirk, G.: 1969, Magnetic Fields and the Structure of the Solar Corona. I: Methods of Calculating Coronal Fields. *Solar Phys.* **9**, 131. DOI. ADS.
- Antiochos, S.K., Linker, J.A., Lionello, R., Mikić, Z., Titov, V., Zurbuchen, T.H.: 2012, The Structure and Dynamics of the Corona–Heliosphere Connection. *Space Sci. Rev.* **172**, 169. DOI. ADS.
- Brooks, D.H., Ugarte-Urra, I., Warren, H.P.: 2015, Full-Sun observations for identifying the source of the slow solar wind. *Nature Communications* **6**, 5947. DOI. ADS.
- Büergi, A., Geiss, J.: 1986, Helium and minor ions in the corona and solar wind - Dynamics and charge states. *Solar Phys.* **103**, 347. DOI. ADS.
- Culhane, J.L., Brooks, D.H., van Driel-Gesztelyi, L., Démoulin, P., Baker, D., DeRosa, M.L., Mandrini, C.H., Zhao, L., Zurbuchen, T.H.: 2014, Tracking Solar Active Region Outflow Plasma from Its Source to the Near-Earth Environment. *Solar Phys.* **289**, 3799. DOI. ADS.
- Delaboudinière, J.-P., Artzner, G.E., Brunaud, J., Gabriel, A.H., Hochedez, J.F., Millier, F., Song, X.Y., Au, B., Dere, K.P., Howard, R.A., Kreplin, R., Michels, D.J., Moses, J.D., Defise, J.M., Jamar, C., Rochus, P., Chauvineau, J.P., Marioge, J.P., Catura, R.C., Lemen, J.R., Shing, L., Stern, R.A., Gurman, J.B., Neupert, W.M., Maucherat, A., Clette, F., Cugnon, P., van Dessel, E.L.: 1995, EIT: Extreme-Ultraviolet Imaging Telescope for the SOHO Mission. *Solar Phys.* **162**, 291. DOI. ADS.
- Domingo, V., Fleck, B., Poland, A.I.: 1995, The SOHO Mission: an Overview. *Solar Phys.* **162**, 1. DOI. ADS.
- Esser, R., Edgar, R.J.: 2000, Reconciling Spectroscopic Electron Temperature Measurements in the Solar Corona with In Situ Charge State Observations. *Astrophys. J. Lett.* **532**, L71. DOI. ADS.
- Feldman, U., Landi, E., Schwadron, N.A.: 2005, On the sources of fast and slow solar wind. *Journal of Geophysical Research (Space Physics)* **110**, 7109. DOI. ADS.

- Fu, H., Xia, L., Li, B., Huang, Z., Jiao, F., Mou, C.: 2014, Measurements of Outflow Velocities in on-disk Plumes from EIS/Hinode Observations. *Astrophys. J.* **794**, 109. DOI. ADS.
- Gloeckler, G., Cain, J., Ipavich, F.M., Tums, E.O., Bedini, P., Fisk, L.A., Zurbuchen, T.H., Bochsler, P., Fischer, J., Wimmer-Schweingruber, R.F., Geiss, J., Kallenbach, R.: 1998, Investigation of the composition of solar and interstellar matter using solar wind and pickup ion measurements with SWICS and SWIMS on the ACE spacecraft. *Space Sci. Rev.* **86**, 497. DOI. ADS.
- Gosling, J.T., Pizzo, V.J.: 1999, Formation and Evolution of Corotating Interaction Regions and their Three Dimensional Structure. *Space Sci. Rev.* **89**, 21. DOI. ADS.
- Habbal, S.R., Esser, R., Arndt, M.B.: 1993, How reliable are coronal hole temperatures deduced from observations? *Astrophys. J.* **413**, 435. DOI. ADS.
- Harra, L.K., Sakao, T., Mandrini, C.H., Hara, H., Imada, S., Young, P.R., van Driel-Gesztelyi, L., Baker, D.: 2008, Outflows at the Edges of Active Regions: Contribution to Solar Wind Formation? *Astrophys. J. Lett.* **676**, L147. DOI. ADS.
- Hassler, D.M., Dammasch, I.E., Lemaire, P., Brekke, P., Curdt, W., Mason, H.E., Vial, J.-C., Wilhelm, K.: 1999, Solar Wind Outflow and the Chromospheric Magnetic Network. *Science* **283**, 810. DOI. ADS.
- Hefti, S., Grünwaldt, H., Bochsler, P., Aellig, M.R.: 2000, Oxygen freeze-in temperatures measured with SOHO/CELIAS/CTOF. *J. Geophys. Res.* **105**, 10527. DOI. ADS.
- Ko, Y.-K., Raymond, J.C., Zurbuchen, T.H., Riley, P., Raines, J.M., Strachan, L.: 2006, Abundance Variation at the Vicinity of an Active Region and the Coronal Origin of the Slow Solar Wind. *Astrophys. J.* **646**, 1275. DOI. ADS.
- Ko, Y.-K., Muglach, K., Wang, Y.-M., Young, P.R., Lepri, S.T.: 2014, Temporal Evolution of Solar Wind Ion Composition and their Source Coronal Holes during the Declining Phase of Cycle 23. I. Low-latitude Extension of Polar Coronal Holes. *Astrophys. J.* **787**, 121. DOI. ADS.
- Kojima, M., Fujiki, K., Ohmi, T., Tokumaru, M., Yokobe, A., Hakamada, K.: 1999, Low-speed solar wind from the vicinity of solar active regions. *J. Geophys. Res.* **104**, 16993. DOI. ADS.
- Krieger, A.S., Timothy, A.F., Roelof, E.C.: 1973, A Coronal Hole and Its Identification as the Source of a High Velocity Solar Wind Stream. *Solar Phys.* **29**, 505. DOI. ADS.
- Krista, L.D., Gallagher, P.T.: 2009, Automated Coronal Hole Detection Using Local Intensity Thresholding Techniques. *Solar Phys.* **256**, 87. DOI. ADS.
- Landi, E., Alexander, R.L., Gruesbeck, J.R., Gilbert, J.A., Lepri, S.T., Manchester, W.B., Zurbuchen, T.H.: 2012a, Carbon Ionization Stages as a Diagnostic of the Solar Wind. *Astrophys. J.* **744**, 100. DOI. ADS.
- Landi, E., Gruesbeck, J.R., Lepri, S.T., Zurbuchen, T.H.: 2012b, New Solar Wind Diagnostic Using Both in Situ and Spectroscopic Measurements. *Astrophys. J.* **750**, 159. DOI. ADS.
- Lepri, S.T., Landi, E., Zurbuchen, T.H.: 2013, Solar Wind Heavy Ions over Solar Cycle 23: ACE/SWICS Measurements. *Astrophys. J.* **768**, 94. DOI. ADS.
- Levine, R.H.: 1982, Open magnetic fields and the solar cycle. I - Photospheric sources of open magnetic flux. *Solar Phys.* **79**, 203. DOI. ADS.
- Li, B., Habbal, S.R., Li, X., Mountford, C.: 2005, Effect of the latitudinal distribution of temperature at the coronal base on the interplanetary magnetic field configuration and the solar wind flow. *Journal of Geophysical Research (Space Physics)* **110**, 12112. DOI. ADS.
- Liewer, P.C., Neugebauer, M., Zurbuchen, T.: 2004, Characteristics of active-region sources of solar wind near solar maximum. *Solar Phys.* **223**, 209. DOI. ADS.
- Luhmann, J.G., Li, Y., Arge, C.N., Gazis, P.R., Ulrich, R.: 2002, Solar cycle changes in coronal holes and space weather cycles. *Journal of Geophysical Research (Space Physics)* **107**, 1154. DOI. ADS.
- Madjarska, M.S., Huang, Z., Doyle, J.G., Subramanian, S.: 2012, Coronal hole boundaries evolution at small scales. III. EIS and SUMER views. *Astron. Astrophys.* **545**, A67. DOI. ADS.
- Mandrini, C.H., Nuevo, F.A., Vásquez, A.M., Démoulin, P., van Driel-Gesztelyi, L., Baker, D., Culhane, J.L., Cristiani, G.D., Pick, M.: 2014, How Can Active Region Plasma Escape into the Solar Wind from Below a Closed Helmet Streamer? *Solar Phys.* **289**, 4151. DOI. ADS.
- Marsch, E.: 2006, Kinetic Physics of the Solar Corona and Solar Wind. *Living Reviews in Solar Physics* **3**, 1. DOI. ADS.
- Mazzotta, P., Mazzitelli, G., Colafrancesco, S., Vittorio, N.: 1998, Ionization balance for optically thin plasmas: Rate coefficients for all atoms and ions of the elements H to NI. *Astron. Astrophys. Suppl.* **133**, 403. DOI. ADS.

- McComas, D.J., Bame, S.J., Barker, P., Feldman, W.C., Phillips, J.L., Riley, P., Griffee, J.W.: 1998, Solar Wind Electron Proton Alpha Monitor (SWEPAM) for the Advanced Composition Explorer. *Space Sci. Rev.* **86**, 563. DOI. ADS.
- Neugebauer, M., Forsyth, R.J., Galvin, A.B., Harvey, K.L., Hoeksema, J.T., Lazarus, A.J., Lepping, R.P., Linker, J.A., Mikić, Z., Steinberg, J.T., von Steiger, R., Wang, Y.-M., Wimmer-Schweingruber, R.F.: 1998, Spatial structure of the solar wind and comparisons with solar data and models. *J. Geophys. Res.* **103**, 14587. DOI. ADS.
- Neugebauer, M., Liewer, P.C., Smith, E.J., Skoug, R.M., Zurbuchen, T.H.: 2002, Sources of the solar wind at solar activity maximum. *Journal of Geophysical Research (Space Physics)* **107**, 1488. DOI. ADS.
- Noci, G., Kohl, J.L., Antonucci, E., Tondello, G., Huber, M.C.E., Fineschi, S., Gardner, L.D., Korendyke, C.M., Nicolosi, P., Romoli, M., Spadaro, D., Maccari, L., Raymond, J.C., Siegmund, O.H.W., Benna, C., Ciaravella, A., Giordano, S., Michels, J., Modigliani, A., Nalletto, G., Panasyuk, A., Pernechele, C., Poletto, G., Smith, P.L., Strachan, L.: 1997, The quiescent corona and slow solar wind. In: Wilson, A. (ed.) *Fifth SOHO Workshop: The Corona and Solar Wind Near Minimum Activity, ESA Special Publication* **404**, 75. ADS.
- Nolte, J.T., Roelof, E.C.: 1973, Large-Scale Structure of the Interplanetary Medium, I: High Coronal Source Longitude of the Quiet-Time Solar Wind. *Solar Phys.* **33**, 241. DOI. ADS.
- Owocki, S.P., Holzer, T.E., Hundhausen, A.J.: 1983, The solar wind ionization state as a coronal temperature diagnostic. *Astrophys. J.* **275**, 354. DOI. ADS.
- Poletto, G.: 2013, Sources of solar wind over the solar activity cycle. *Journal of Advanced Research* **4**, 215. DOI. ADS.
- Richardson, I.G., Cane, H.V.: 2004, Identification of interplanetary coronal mass ejections at 1 AU using multiple solar wind plasma composition anomalies. *Journal of Geophysical Research (Space Physics)* **109**, 9104. DOI. ADS.
- Riley, P., Linker, J.A., Mikić, Z., Lionello, R., Ledvina, S.A., Luhmann, J.G.: 2006, A Comparison between Global Solar Magnetohydrodynamic and Potential Field Source Surface Model Results. *Astrophys. J.* **653**, 1510. DOI. ADS.
- Sakao, T., Kano, R., Narukage, N., Kotoku, J., Bando, T., DeLuca, E.E., Lundquist, L.L., Tsuneta, S., Harra, L.K., Katsukawa, Y., Kubo, M., Hara, H., Matsuzaki, K., Shimojo, M., Bookbinder, J.A., Golub, L., Korreck, K.E., Su, Y., Shibasaki, K., Shimizu, T., Nakatani, I.: 2007, Continuous Plasma Outflows from the Edge of a Solar Active Region as a Possible Source of Solar Wind. *Science* **318**. DOI. ADS.
- Schatten, K.H., Wilcox, J.M., Ness, N.F.: 1969, A model of interplanetary and coronal magnetic fields. *Solar Phys.* **6**, 442. DOI. ADS.
- Schrijver, C.J., De Rosa, M.L.: 2003, Photospheric and heliospheric magnetic fields. *Solar Phys.* **212**, 165. DOI. ADS.
- Schwenn, R.: 2006, Solar Wind Sources and Their Variations Over the Solar Cycle. *Space Sci. Rev.* **124**, 51. DOI. ADS.
- Sheeley, N.R., Wang, Y.-M., Hawley, S.H., Brueckner, G.E., Dere, K.P., Howard, R.A., Koomen, M.J., Korendyke, C.M., Michels, D.J., Paswaters, S.E., Socker, D.G., St. Cyr, O.C., Wang, D., Lamy, P.L., Llebaria, A., Schwenn, R., Simnett, G.M., Plunkett, S., Biesecker, D.A.: 1997, Measurements of Flow Speeds in the Corona Between 2 and 30 R. *Astrophys. J.* **484**, 472. ADS.
- Smith, C.W., L'Heureux, J., Ness, N.F., Acuña, M.H., Burlaga, L.F., Scheifele, J.: 1998, The ACE Magnetic Fields Experiment. *Space Sci. Rev.* **86**, 613. DOI. ADS.
- Snyder, C.W., Neugebauer, M.: 1966, The Relation of Mariner-2 Plasma Data to Solar Phenomena. In: Mackin, R.J. Jr., Neugebauer, M. (eds.) *The Solar Wind*, 25. ADS.
- Stone, E.C., Frandsen, A.M., Mewaldt, R.A., Christian, E.R., Margolies, D., Ormes, J.F., Snow, F.: 1998, The Advanced Composition Explorer. *Space Sci. Rev.* **86**, 1. DOI. ADS.
- Subramanian, S., Madjarska, M.S., Doyle, J.G.: 2010, Coronal hole boundaries evolution at small scales. II. XRT view. Can small-scale outflows at CHBs be a source of the slow solar wind. *Astron. Astrophys.* **516**, A50. DOI. ADS.
- Suess, S.T., Wang, A.-H., Wu, S.T., Nerney, S.F.: 1999, Streamer Evaporation. *Space Sci. Rev.* **87**, 323. DOI. ADS.
- Tu, C.-Y., Zhou, C., Marsch, E., Xia, L.-D., Zhao, L., Wang, J.-X., Wilhelm, K.: 2005, Solar Wind Origin in Coronal Funnels. *Science* **308**, 519. DOI. ADS.
- van Driel-Gesztelyi, L., Culhane, J.L., Baker, D., Démoulin, P., Mandrini, C.H., DeRosa, M.L., Rouillard, A.P., Opitz, A., Stenborg, G., Vourlidas, A., Brooks, D.H.: 2012, Magnetic Topology of Active Regions and Coronal Holes: Implications for Coronal Outflows and the Solar Wind. *Solar Phys.* **281**, 237. DOI. ADS.

-
- Wang, Y.-M., Sheeley, N.R. Jr.: 1990, Solar wind speed and coronal flux-tube expansion. *Astrophys. J.* **355**, 726. DOI. ADS.
- Wang, Y.-M., Sheeley, N.R. Jr.: 2003, The Solar Wind and Its Magnetic Sources at Sunspot Maximum. *Astrophys. J.* **587**, 818. DOI. ADS.
- Wang, Y.-M., Ko, Y.-K., Grappin, R.: 2009, Slow Solar Wind from Open Regions with Strong Low-Coronal Heating. *Astrophys. J.* **691**, 760. DOI. ADS.
- Wang, Y.-M., Sheeley, N.R. Jr., Walters, J.H., Brueckner, G.E., Howard, R.A., Michels, D.J., Lamy, P.L., Schwenn, R., Simnett, G.M.: 1998, Origin of Streamer Material in the Outer Corona. *Astrophys. J. Lett.* **498**, L165. DOI. ADS.
- Xia, L.D., Marsch, E., Curdt, W.: 2003, On the outflow in an equatorial coronal hole. *Astron. Astrophys.* **399**, L5. DOI. ADS.
- Zhao, L., Landi, E.: 2014, Polar and Equatorial Coronal Hole Winds at Solar Minima: From the Heliosphere to the Inner Corona. *Astrophys. J.* **781**, 110. DOI. ADS.
- Zhao, L., Zurbuchen, T.H., Fisk, L.A.: 2009, Global distribution of the solar wind during solar cycle 23: ACE observations. *Geophys. Res. Lett.* **36**, 14104. DOI. ADS.
- Zharkova, V.V., Aboudarham, J., Zharkov, S., Ipson, S.S., Benkhalil, A.K., Fuller, N.: 2005, Solar Feature Catalogues In Egso. *Solar Phys.* **228**, 361. DOI. ADS.
- Zirker, J.B.: 1977, Coronal holes and high-speed wind streams. *Reviews of Geophysics and Space Physics* **15**, 257. DOI. ADS.
- Zurbuchen, T.H.: 2001, Heliospheric Magnetic Field Configuration and its Coronal Sources. In: Brekke, P., Fleck, B., Gurman, J.B. (eds.) *Recent Insights into the Physics of the Sun and Heliosphere: Highlights from SOHO and Other Space Missions*, IAU Symposium **203**, 585. ADS.
- Zurbuchen, T.H., Hefti, S., Fisk, L.A., Gloeckler, G., Schwadron, N.A.: 2000, Magnetic structure of the slow solar wind: Constraints from composition data. *J. Geophys. Res.* **105**, 18327. DOI. ADS.

Table 1. Number of daily solar wind samples analyzed in each year.

Year	All sources	CH winds	AR winds	QS winds	Undefined
1999	237 (188)	32 (27)	148 (117)	28 (23)	29 (21)
2000	261 (221)	50 (47)	145 (125)	36 (28)	30 (21)
2001	272 (220)	43 (39)	155 (119)	38 (30)	36 (32)
2002	289 (259)	65 (62)	152 (135)	38 (35)	34 (27)
2003	277 (259)	142 (138)	71 (65)	34 (32)	30 (24)
2004	242 (211)	63 (61)	94 (81)	34 (30)	51 (39)
2005	250 (201)	78 (70)	70 (61)	56 (34)	46 (36)
2006	262 (200)	60 (56)	55 (43)	94 (62)	53 (39)
2007	257 (178)	68 (57)	36 (30)	114 (59)	39 (32)
2008	259 (187)	61 (58)	29 (27)	157 (92)	12 (10)
Sum	2606 (2124)	662 (615)	955 (803)	629 (425)	360 (281)

Table 2. Number of daily slow solar wind samples analyzed in each year.

Year	All sources	CH winds	AR winds	QS winds	Undefined
1999	188 (141)	20 (15)	119 (89)	23 (18)	26 (19)
2000	204 (167)	26 (23)	123 (103)	29 (23)	26 (18)
2001	245 (194)	37 (34)	139 (103)	37 (29)	32 (28)
2002	238 (208)	40 (37)	135 (118)	32 (29)	31 (24)
2003	111 (96)	35 (31)	36 (32)	20 (18)	20 (15)
2004	194 (163)	36 (34)	83 (70)	28 (24)	47 (35)
2005	172 (132)	34 (29)	52 (44)	47 (28)	39 (31)
2006	205 (146)	38 (34)	40 (28)	81 (50)	46 (34)
2007	187 (116)	38 (28)	30 (25)	91 (42)	28 (21)
2008	169 (102)	25 (22)	15 (13)	122 (61)	7 (6)
Sum	1913 (1465)	329 (287)	772 (625)	510 (322)	302 (231)

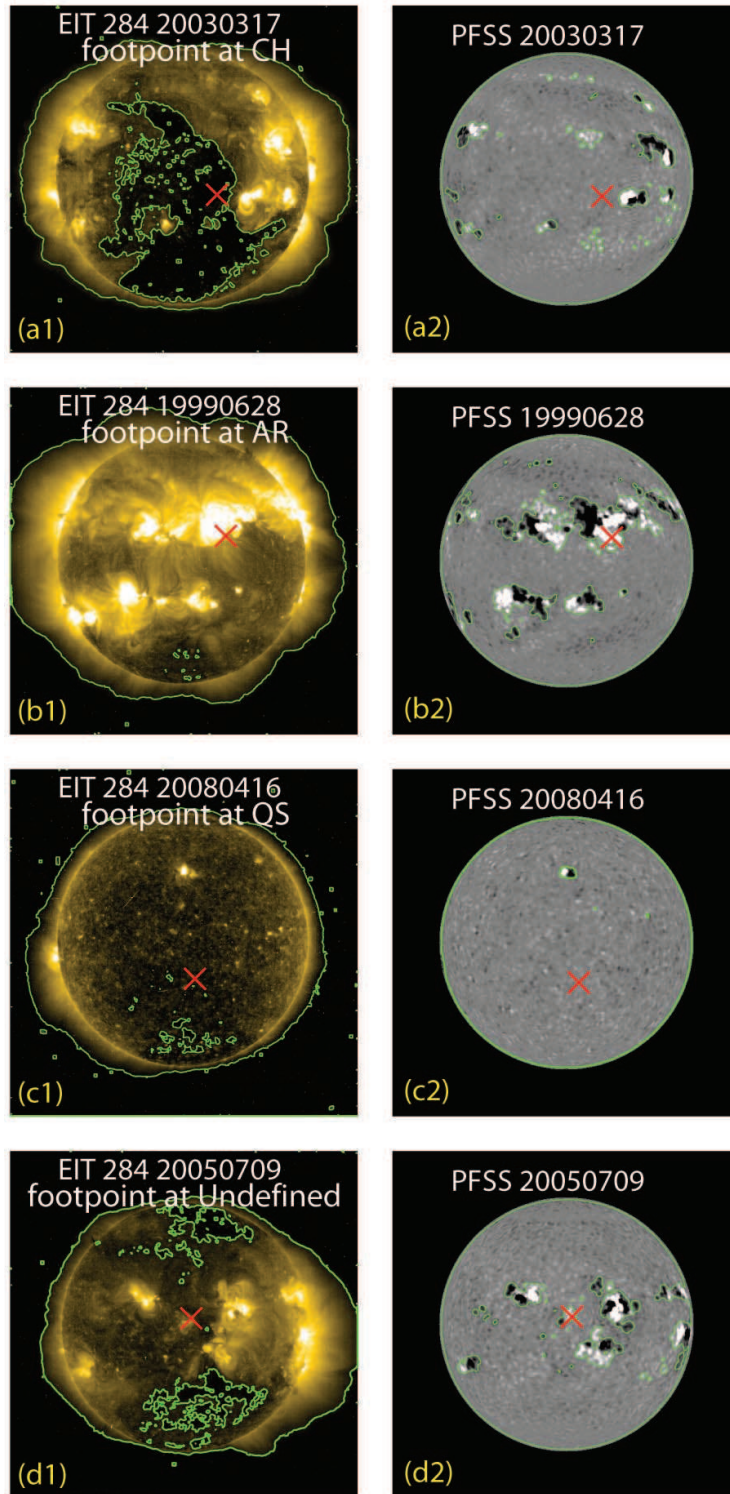


Figure 1. Illustration of the classification scheme of the ACE solar winds. The footpoints of the solar wind flow tubes are given by the red crosses, which are classified as being associated with a coronal hole (the first row), an active region (second), the quiet Sun (third) and some undefined source (bottom). The left column presents the EIT 284 Å images, while the right column gives the corresponding magnetic morphology of the photosphere. The green contours outline CH (left column) and Magnetically Concentrated Area (MCA) boundaries (right). An animation showing the sources during 1999–2008 is available online.

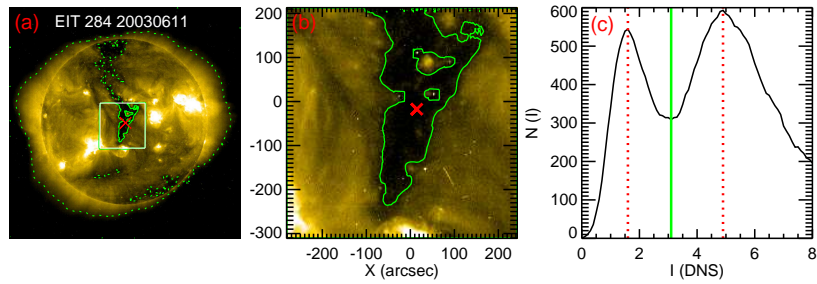


Figure 2. The scheme for outlining coronal holes. Panel (a) presents the EIT 284 image on 2003 June 11, when the traced-back footpoint (the red cross) is located close to a low-latitude CH. The white box encloses the region for which the intensity histogram is constructed and presented in panel (c), where the solid green line represents the minimum between the two peaks, given by the two red dotted lines. This minimum is used as the threshold to delineate CH boundaries in (a), where the contours inside (outside) the box are given by the solid (dotted) lines. Panel (b) is an enlarged version of the part enclosed by the box in (a).

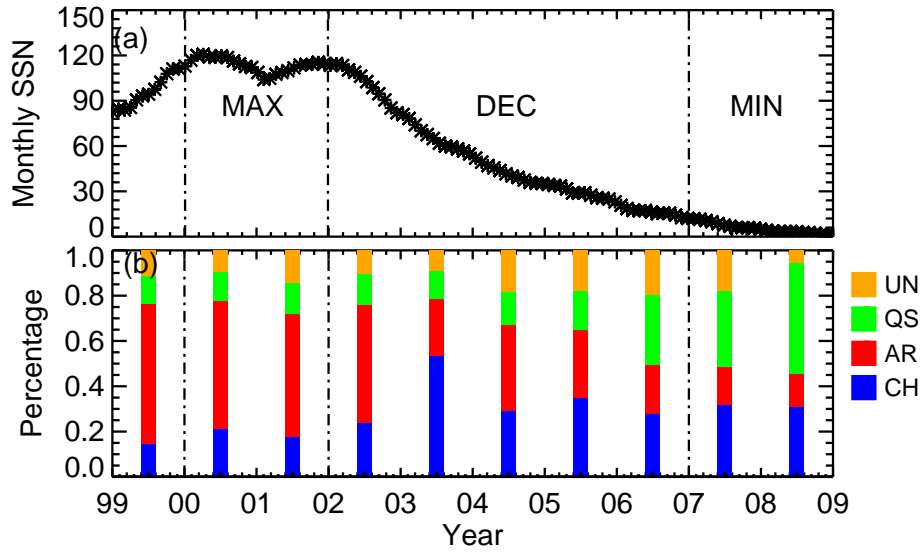


Figure 3. Fractions of the ACE winds with different sources as a function of time. Panel (a) shows the temporal evolution of the smoothed monthly sunspot number during 1999-2008, which is further divided into the maximum (labeled MAX), declining (DEC) and minimum (MIN) phases. Panel (b) gives the percentage of the coronal hole (CH, blue), active region (AR, red), quiet Sun (QS, green) and undefined (UN, orange) winds.

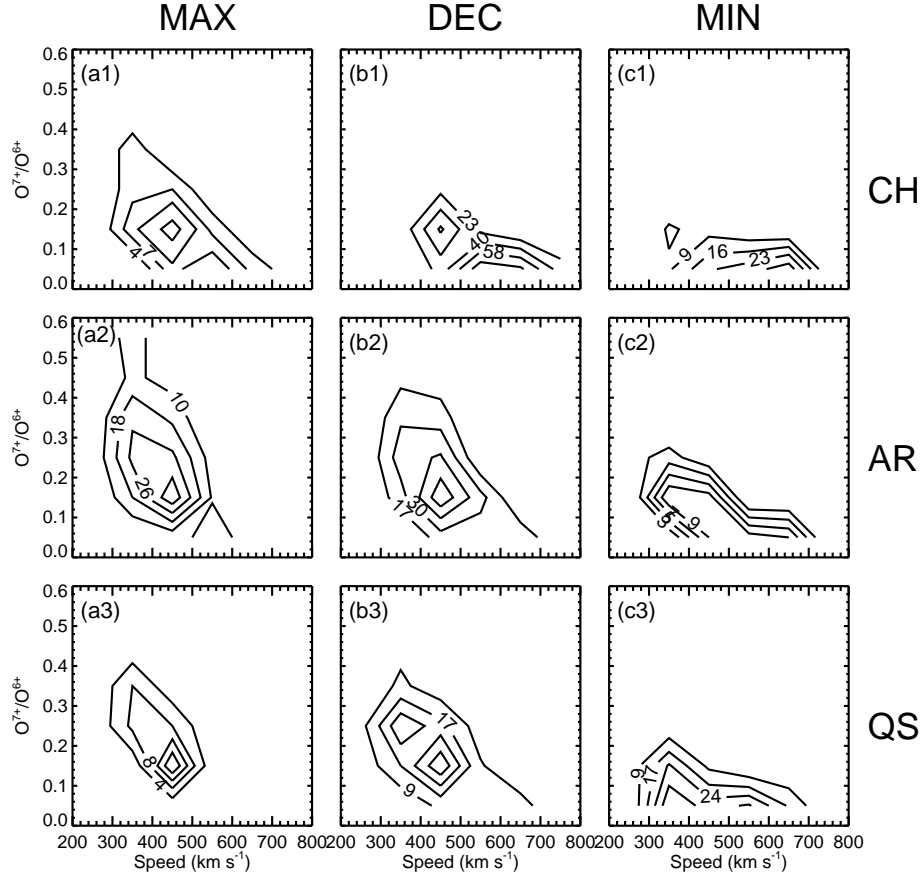


Figure 4. Dependence on solar activity of the distribution of solar winds from different sources in the speed– O^{7+}/O^{6+} space. The left (middle, right) column corresponds to the maximum (declining, minimum) phase, while the first (second, third) row represents the winds from coronal holes (active regions, the quiet Sun). Here the counts of solar wind samples in different groups are shown as contour plots with the contours equally spaced in each panel.

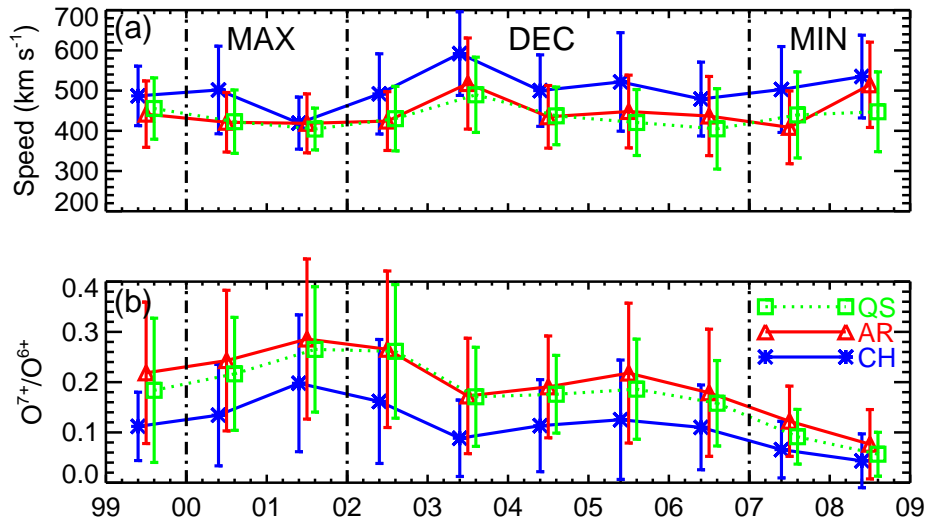


Figure 5. In situ properties of solar winds from different sources as a function of time during 1999–2008. Here panels (a) and (b) are for the wind speeds and O^{7+}/O^{6+} ratios, respectively. The interval between 2000 and 2008 is further divided into three activity phases: maximum (MAX), declining (DEC) and minimum (MIN). The winds from coronal holes (CHs), active regions (ARs) and the quiet Sun (QS) are represented by the blue, red, and green curves, respectively. As for the error bars, they represent the standard deviations in each year.

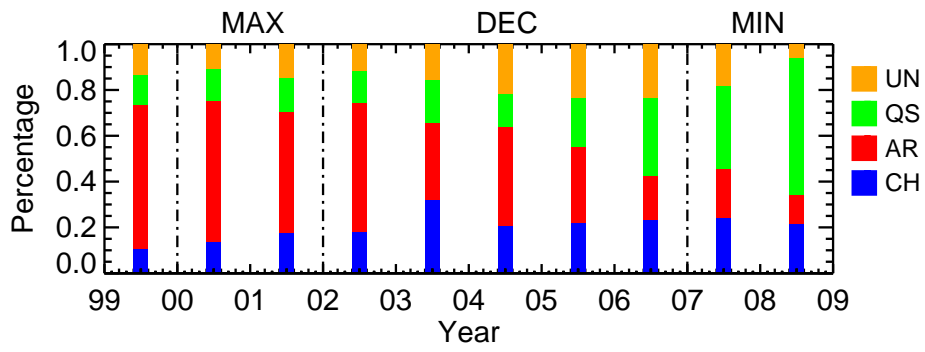


Figure 6. Similar to Figure 3 but restricted to the slow wind with speeds less than 500km s^{-1} .

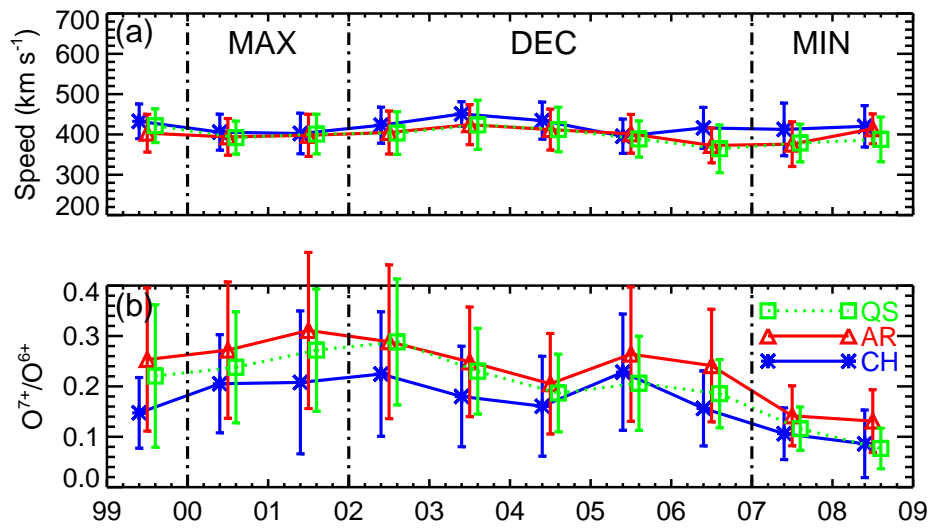


Figure 7. Similar to Figure 5 but restricted to the slow wind.